Field Guide to

Solar Optics

Julius Yellowhair

SPIE Field Guides
Volume FG47

J. Scott Tyo, Series Editor

SPIE PRESS
Bellingham, Washington USA

Library of Congress Cataloging-in-Publication Data

Names: Yellowhair, Julius E., author.
Title: Field guide to solar optics / Julius Yellowhair.
Description: Bellingham, Washington : SPIE Press, [2020] | Includes bibliographical references and index.
Identifiers: LCCN 2020009994 | ISBN 9781510636972 (spiral bound) | ISBN 9781510636989 (pdf)
Subjects: LCSH: Solar collectors–Optical properties. | Solar energy.
Classification: LCC TJ812 .Y45 2020 | DDC 621.47/2–dc23
LC record available at https://lccn.loc.gov/2020009994

Published by

SPIE
P.O. Box 10
Bellingham, Washington 98227-0010 USA
Phone: 360.676.3290
Fax: 360.647.1445
Email: Books@spie.org
Web: www.spie.org

Copyright © 2020 Society of Photo-Optical Instrumentation Engineers (SPIE)

All rights reserved. No part of this publication may be reproduced or distributed in any form or by any means without written permission of the publisher.

The content of this book reflects the thought of the author. Every effort has been made to publish reliable and accurate information herein, but the publisher is not responsible for the validity of the information or for any outcomes resulting from reliance thereon.

Printed in the United States of America.
First printing.
For updates to this book, visit http://spie.org and type “FG47” in the search field.

Table of Contents

Table of Contents

Table of Contents

Table of Contents

Field Guide to Solar Optics

The *Field Guide to Solar Optics* consolidates and summarizes optical topics in solar technologies and engineering that are dispersed throughout literature. It also attempts to clarify topics and terms that could be confusing or at times misused.

As with any technology area, optics related to solar technologies can be a wide-ranging field. The topics selected for this field guide are those frequently encountered in solar engineering and research for energy harvesting, particularly for electricity generation. Therefore, the selected topics are slanted toward solar thermal power, or as it is commonly called, concentrating solar power.

The first section provides background on energy needs and usage, and explains where solar technologies fit into the energy mix. Section 2 covers properties of the sun and presents our basic understanding of solar energy collection. The third section introduces optical properties, concepts, and basic components. In Section 4, the various optical systems used in solar engineering are described. Optical systems used for solar energy collection are commonly referred to as collectors (e.g., a collector field)—a term that is frequently used in this field guide. Another term commonly applied in solar collectors is nonimaging optics. The fifth section introduces concepts for characterizing optical components/systems and analysis approaches. Lastly, the measurement tools commonly used in solar engineering and research are described in Section 6.

The fundamentals of each topic are covered. Providing methods or approaches to designs was not the goal of this field guide. However, the fundamental understanding that can be gained from the book can be extended and used for design of components and systems.

Julius Yellowhair
June 2020

Energy Usage and Needs

The world needs energy to function and move societies forward. Access to adequate and reliable energy resources is crucial for economic growth and for maintaining the quality of our lives. As our need for energy continues to grow, one important question to ask is whether current levels of **energy consumption** and production are sustainable. The United States (U.S.) Energy Information Administration (EIA) publishes energy data periodically. The graph shows the world energy consumption from different energy sources, starting from 1990 and projected to 2040. This includes all of the energy consumed (fuel for transportations, electricity, etc.).

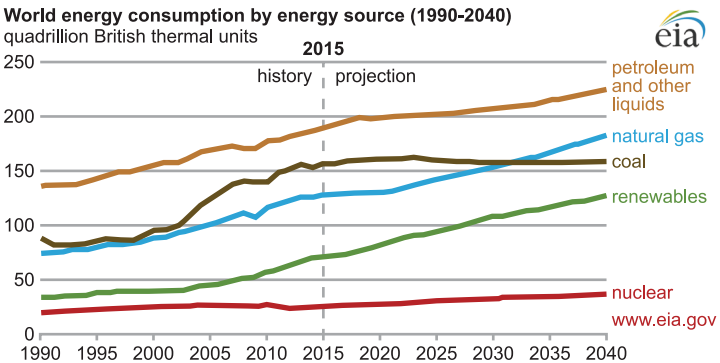

Oil continues to be the largest resource for our **energy needs**. However, oil supplies are finite, and it is believed that its use contributes to climate change. Coal usage has seen an increase in recent years. Coal is also finite in supply and also could be contributing to climate change.

Renewable energy sources have been growing rapidly in the last decade and, according to the figure above, will continue to grow in the future and outpace other energy sources.

Developed countries, including the U.S., have plans to increase renewable sources into their energy portfolios to meet some of our growing demands for energy and to produce cleaner energy.

Concentrating Solar Technologies

Concentrating solar power (CSP), sometimes called **solar thermal power**, utilizes the *thermal energy of the sun*, which is converted into mechanical energy to produce electricity. Solar energy is collected and concentrated on receivers using large collectors (i.e., mirrors or other reflective surfaces). Receivers composed of metal tubes flow a heat transfer fluid (HTF) that is heated by the concentrated solar power. The hot fluid (water, oil, or molten salt) is transferred to the **power block**, where water is heated to generate steam, which then runs a turbine to generate electricity. Some of the hot fluid can be stored for later use or cloudy days. This is called **thermal energy storage**. There are three main types of CSP technologies: parabolic trough, power tower, and dish-engine systems. A schematic of each type is shown below.

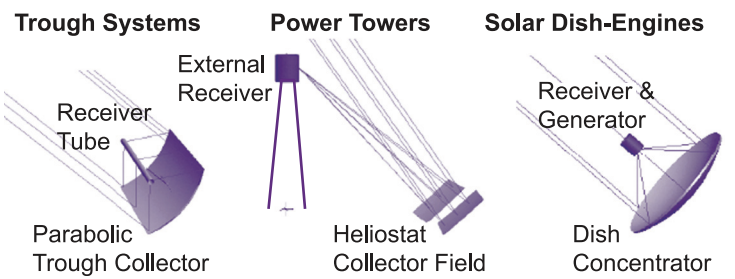

The Solar Energy Generating Systems (SEGS) power plants near Barstow, California utilize the parabolic trough technology and are the longest-running CSP plants in the world (commissioned in the mid-1980s). There are nine plants in total, generating 361 MW.

Ivanpah and Crescent Dunes plants in Nevada are large power tower plants commissioned in 2014 and 2015. Ivanpah has three power tower units producing at a capacity of 392 MW. Crescent Dunes has one central tower producing at a capacity of 110 MW with 10 h of thermal energy storage.

The last parabolic dish project in the U.S. was a 1.5 MW plant in Maricopa, Arizona in 2009.

Earth Orbit

The earth orbits the sun in an elliptical path at a speed of 108,000 km/h (67,108 mph) and with **eccentricity** of 0.0167. It completes one **orbit** every 365.256 days (1 sidereal year). The extra partial day accumulates to a full day every four years, creating what is known as a leap year.

The planet's distance from the sun varies as it orbits. At perihelion, around 3 January, the earth is closest to the sun when the distance is about 147,098,074 km. At aphelion, around 3 July, it is farthest from the sun when the distance is about 152,097,701 km. The average distance between the earth and the sun is about 149.6 million km, or one **astronomical unit** [AU]. The changing seasons are determined by the tilt of the earth's rotation axis, not its distance from the sun. Because of the **axial tilt** of the earth, the highest solar energy is incident at 23.4 deg north of the equator at the summer solstice (Tropic of Cancer) and 23.4 deg south of the equator at the winter solstice (Tropic of Capricorn).

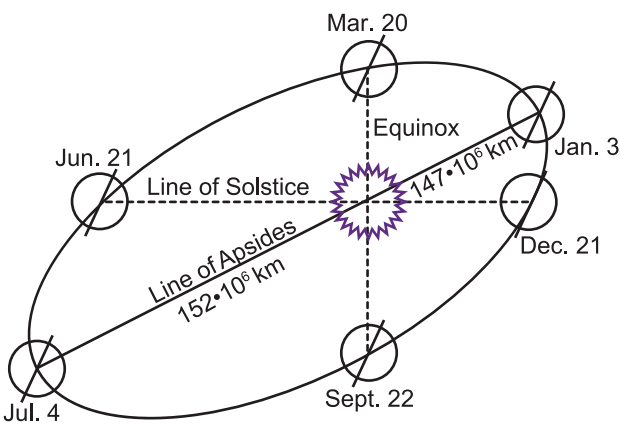

As seen from Earth, the planet's **orbital prograde motion** (i.e., earth's rotation direction) makes the sun appear to move with respect to other stars at a rate of about 1 deg (or a sun or moon diameter) every 12 h eastward per solar day based on the earth's orbital speed.

Solar Radiation Energy

Radiation is emitted at the speed of light but can be emitted at different energy levels. The photon energy Q_e can be defined in terms of the radiation **frequency** ν or **wavelength** λ:

$$Q_e = h\nu = h\frac{c}{\lambda}$$

where h is **Planck's constant**, and c is the speed of light. To find the photon energy in electronvolts [eV], the following approximation can be used with the wavelength specified in microns (μm):

$$Q_e = \frac{1.2398}{\lambda\,[\mu\text{m}]}\ \text{eV}$$

The different energy regimes are usually depicted on the **electromagnetic** (EM) **spectrum**, as shown below, where the frequency, and therefore the energy, increases to the left. The wavelength, however, reduces to the left since it is inversely proportional to the energy.

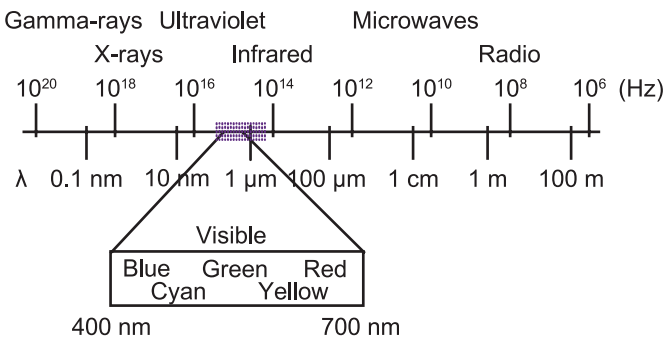

From the **solar spectrum** most of the sun's energy on Earth is between 280 nm and 2.5 μm (ultraviolet to infrared), marked by the shaded region in the EM spectrum diagram above. Over the solar spectrum, the sun emits mostly in the **visible region** (400 to 700 nm).

Solar Radiation Metrology

Two instruments are primarily used to measure solar radiation for direct normal irradiance (DNI), **global horizontal irradiance** (GHI), and **global tilted irradiance** (GTI). A **pyrheliometer** is an instrument for measuring direct beam solar irradiance. Sunlight enters the instrument through a window and is directed onto a thermopile or thermocouple, which converts heat to an electrical signal that can be recorded. The signal voltage is converted via a formula to measure irradiance [W/m^2]. A pyrheliometer is used with a solar tracking system to keep the instrument aimed at the sun.

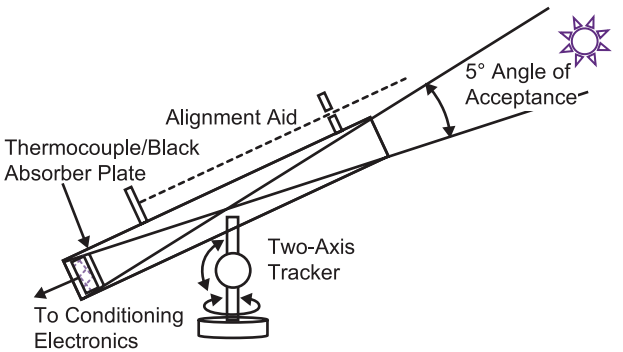

Similarly, a **pyranometer** uses thermopiles or thermocouples to measure solar irradiance [W/m^2] on a planar surface over a hemisphere. Direct sunlight and diffuse sunlight enter the glass hemispheric dome and arrive at an array of temperature sensors. The temperature is then converted to an electrical signal, and the signal is calibrated to provide an irradiance measurement. When the pyranometer is placed on a level surface, it measures GHI. When placed on a tilted surface, it measures GTI.

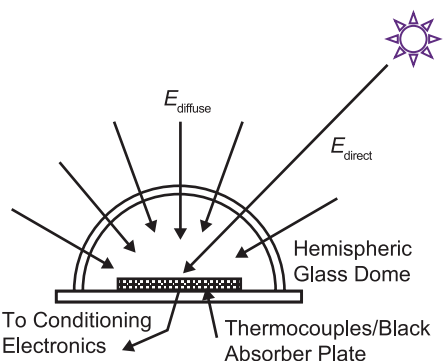

Radiometry Basics

Radiant exitance M [W/m^2] is the radiation emitted by a source of area A, whereas **irradiance** E [W/m^2] is radiation incident on a target surface of area A.

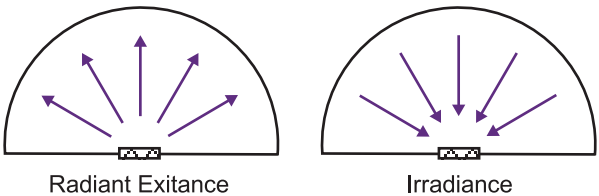

Irradiance E can be written as

$$E = \frac{d\Phi}{dA}$$

Radiant exitance is defined in the same way. The difference is in the direction of the radiation.

The **radiant flux** or power Φ [W] is calculated as the integration of irradiance (or radiant exitance) over the collection area:

$$\Phi = \int E\, dA$$

Radiation (emitted or incident) can be bounded by a surface of area A.

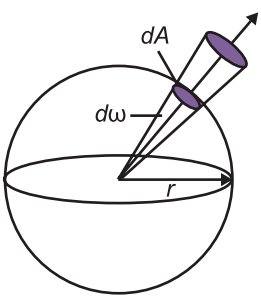

Radiation can also be defined over a **solid angle** ω. A solid angle is defined as

$$d\omega = \frac{dA}{r^2} = \sin\theta d\theta\, d\phi$$

$$\omega = \int_{\phi}\int_{\theta} \sin\theta d\theta\, d\phi$$

The **projected solid angle** Ω is the projection of the solid angle ω onto the observer plane and is defined as

$$d\Omega = \cos\theta\, d\omega$$

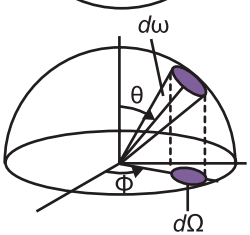

Solar Collector Basics

In solar thermal systems, **solar collectors** (i.e., mirrors) are the fundamental components needed to collect and concentrate solar radiation onto a receiver or heat-absorbing element(s).

A typical solar collector mirror facet has the so-called sandwich construction.

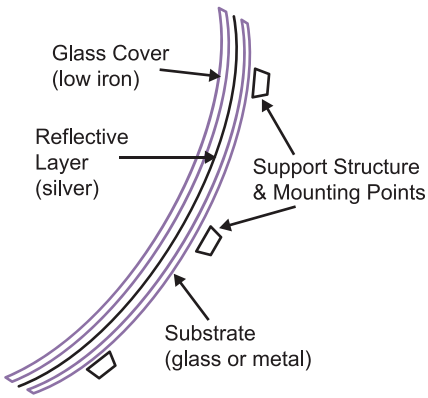

This refers to the way the mirror facets are constructed. Two glass sheets "sandwich" the reflective film. One glass sheet serves as the substrate, and the other serves as the front cover. The glass sheets are on the order of 1–5 mm thick. The reflective film is typically silver because silver reflects well over the **solar spectrum** (discussed on page 41).

The mirror, which is on the order of 1–3 m^2 in size, can nominally be flat or curved, depending on the solar technology application. The glass assembly is bonded to a support structure that can be a metal framework, stamped sheet metal, honeycomb panels, or another stiff structure. Mounting points are then bonded to the structure and serve as the interface points to the large collector frame. Three mounting points are ideal if two-axis mirror facet angle adjustments are needed. Additional mounting points can induce stress on the mirror facet. During facet angle adjustments, or **canting**, one mounting point serves as the pivot point, while the other mounting points are adjusted with actuators to tilt the mirror into alignment. A rigid collector frame, such as a heliostat frame, can hold an array of the mirror facets. The mirror array is arranged such that it will concentrate the sunlight onto a target or receiver.

Linear Collectors

Linear collectors are curved in one direction and usually have a rectangular aperture. Because they are curved only in one direction, they focus the incident sunlight to a line. The **parabolic trough concentrator** is an example of a linear collector. The curved cross-section follows a parabolic shape of the form

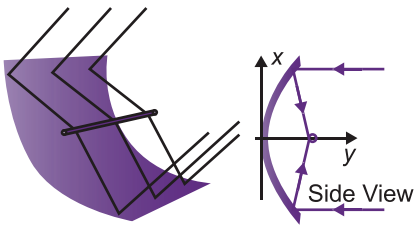

$$y = \frac{x^2}{4f}$$

where f is the focal length of the parabolic shape. The rim angle can be calculated as

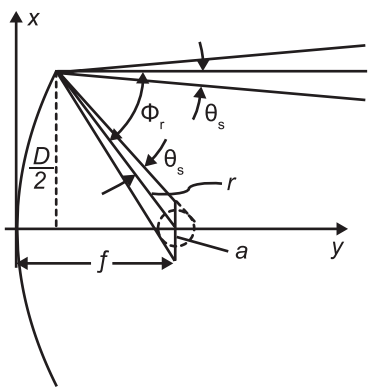

$$\phi_r = \tan^{-1}\left[\frac{8(f/D)}{16(f/D)^2 - 1}\right] = \sin^{-1}\left(\frac{D}{2r}\right)$$

The concentration C on a flat surface at the focal point perpendicular to the optical axis can be determined by considering only the angle beam spread from the sun:

$$C = \frac{a}{D} = \frac{1}{2\sin(\theta_s)}$$

which shows half the maximum solar concentration C_{max} possible for an ideal linear concentrator. A circular receiver is shown as a dashed circle. The size is just big enough to intercept rays from an ideal concentrator. Imperfections from the reflector (i.e., slope errors) will cause the reflected beam to spread farther, which will require a slightly larger receiver size to minimize light spillage.

Linear Fresnel concentrators also fall into the linear concentrator category.

Combined Optical Errors

The collector **tracking error** can be defined as

$$\sigma_{\text{tracking}} = \sqrt{\Delta\theta^2 + \Delta\alpha^2}$$

where the errors in the azimuth and elevation axes are combined. All **optical errors** are assumed to follow normal or Gaussian distributions. That is, when the errors from all of the collectors (e.g., heliostats) are combined, the distribution of the errors will tend to follow Gaussian distributions. The probability distribution function for each error source can be defined as

$$p = e^{-\frac{(x-x_0)^2}{2\sigma^2}}$$

The different error sources can be combined through a convolution calculation:

$$P = p_1 * p_2 * \ldots$$

The error sources can be combined as a root sum square:

$$\sigma_{\text{optical\_total}} = \sqrt{\sigma^2_{\text{surface}} + \sigma^2_{\text{canting}} + \sigma^2_{\text{tracking}} + \sigma^2_{\text{wind}} + \sigma^2_{\text{gravity}}}$$

The beam reflected from the collectors will spread due to these error sources and the sun angular spread.

The total reflected beam angular spread can be calculated as

$$\sigma_{\text{beam\_spread\_total}} = \sigma_{\text{optical\_total}} + \sigma_{\text{sunshape}}$$

The **sunshape** is sometimes included in the convolution calculation. Here, it is merely added to the result of the convolution calculation since sunshape is a systematic "error" source. Also, $\sigma_{\text{optical\_total}}$ is one standard deviation wide. To include more of the beam spread from the optical errors, $N\sigma_{\text{optical\_total}}$ can be used, where N is the number of standard deviations ($N = 1$, 2, or 3).

Laser Scanning System

A **laser scanning system** was developed and implemented by Sandia and NREL[8] for reflector surface characterization. The system uses a laser to scan the reflector surface; the laser beam is reflected back to a target, and a camera is used to detect the location of the laser spot. Individual mirror facets or entire collector systems can be measured with this method.

A test is performed by placing the reflective surface at roughly twice its **focal length** from the laser scanner and target board so that the reflected laser beam lands on the target board. The laser is steered by scanning mirrors. The location of the return spot is measured with a **CCD camera**. This process is repeated across the surface of the test article in a user-defined pattern. From the scanner aiming angles and return spot locations, the slope at each point and the shape of the mirror surface are computed using predefined coordinate definitions. Surface slope deviations from the ideal surface can be determined.

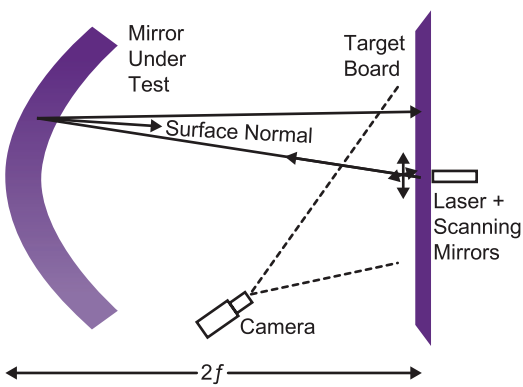

To test flat reflective surfaces, the target board size must be increased to slightly larger than twice the size of the mirror under test to capture all of the reflected light.

The camera calibration involves temporarily mounting a rectangular grid of spots with known spacing on the target board, and collecting images of the target grid with the camera. The centroids of each circular spot are determined to a fraction of a pixel, and a fit of the surface is performed. This surface fit is possible because the actual grid spacing in both X and Y directions is known.

Emissometers

An **emissometer** works according to the same principles as a reflectometer but measures the in-band reflectance on samples that are all in the IR, which it then uses to calculate the thermal emittance of the samples. The **conservation of energy** states that the sum of the transmitted, reflected, and absorbed light in all directions and at all wavelengths must equal unity, or

$$\tau + \rho + \alpha = 1$$

The **directional emittance** becomes

$$\varepsilon_d = 1 - \rho_d - \tau_s$$

for transmissive surfaces, where ρ_d is the measured directional reflectance. For opaque surfaces, the transmittance component τ_s is zero. The total directional emittance of an opaque surface at a given temperature is

$$\varepsilon_T(\theta, \phi) = 1 - \frac{\int_0^\infty \rho_d(\lambda) u(\lambda, T) d\lambda}{\int_0^\infty u(\lambda, T) d\lambda}$$

where u is **Planck's function** in terms of spectral energy density at a given temperature:

$$u(\lambda, T) = \frac{8\pi hc}{\lambda^5 (e^{hc/\lambda kT} - 1)}$$

When the sample reflectance is measured over several incidence angles, the total **hemispherical emittance** can be estimated by

$$\varepsilon_H = 2 \int_0^{\pi/2} \varepsilon_T(\theta) \sin\theta \cos\theta \, d\theta$$

Emissometers provide measurements at room temperature but calculate the emittance at the specified temperature. Like commercial reflectometers, portable emissometers are also commercially available.

Equation Summary

Atmospheric attenuation (Schmitz):

$$\eta_{\text{atm}} = \begin{cases} 0.99321 - 0.0001176\,R + 1.97 \cdot 10^{-8}\,R^2 & R \le 1\,\text{km} \\ \exp(-0.000106\,R) & R > 1\,\text{km} \end{cases}$$

Cassegrain system parameters (radii of curvature):

$$R_1 = \frac{2DF}{F - B}$$

$$R_2 = \frac{2DB}{F - B - D}$$

Circle surface equation:

$$(y - r)^2 + x^2 = r^2$$

Collector field efficiency:

$$\eta_{\text{field}} = \frac{\sum_{i=1}^{N_h} \eta(i)}{N_h}$$

where N_h is the total number of heliostats in the field.

Collector optical efficiency:

$$\eta_{\text{opt}} = \eta_{\text{sb}} \cdot \eta_{\cos} \cdot \eta_{\text{int}} \cdot \eta_{\text{ref}} \cdot \eta_{\text{atm}}$$

$$\eta(i) = \frac{\sum_{n=1}^{365} \int_{t_0}^{t_1} \eta(t)\,dt}{\sum_{n=1}^{365} \int_{t_0}^{t_1} dt}$$

$$\eta_E(i) = \frac{\sum_{n=1}^{365} \int_{t_0}^{t_1} E(t)\eta(t)\,dt}{\sum_{n=1}^{365} \int_{t_0}^{t_1} E(t)\,dt}$$

Concentration limits:

$$\text{Linear concentrators}: C_{\max} = \frac{R}{r_s} = \frac{1}{\sin\theta_s}$$

$$\text{Point concentrators}: C_{\max} = \left(\frac{R}{r_s}\right)^2 = \frac{1}{\sin^2\theta_s}$$